Soheila Zeinali[1]
Barbaros Çetin[1]
Samad Nadimi Bavil Oliaei[2]
Yiğit Karpat[2,3]

[1]Mechanical Engineering Department, Microfluidics and Lab-on-a-chip Research Group, Bilkent University, Ankara, Turkey
[2]Mechanical Engineering Department, Microsystem Design and Manufacturing Center, Bilkent University, Ankara, Turkey
[3]Industrial Engineering Department, Bilkent University, Ankara, Turkey

Received October 15, 2014
Revised January 26, 2015
Accepted February 15, 2015

Research Article

Fabrication of continuous flow microfluidics device with 3D electrode structures for high throughput DEP applications using mechanical machining

Microfluidics is the combination of micro/nano fabrication techniques with fluid flow at microscale to pursue powerful techniques in controlling and manipulating chemical and biological processes. Sorting and separation of bio-particles are highly considered in diagnostics and biological analyses. Dielectrophoresis (DEP) has offered unique advantages for microfluidic devices. In DEP devices, asymmetric pair of planar electrodes could be employed to generate non-uniform electric fields. In DEP applications, facing 3D sidewall electrodes is considered to be one of the key solutions to increase device throughput due to the generated homogeneous electric fields along the height of microchannels. Despite the advantages, fabrication of 3D vertical electrodes requires a considerable challenge. In this study, two alternative fabrication techniques have been proposed for the fabrication of a microfluidic device with 3D sidewall electrodes. In the first method, both the mold and the electrodes are fabricated using high precision machining. In the second method, the mold with tilted sidewalls is fabricated using high precision machining and the electrodes are deposited on the sidewall using sputtering together with a shadow mask fabricated by electric discharge machining. Both fabrication processes are assessed as highly repeatable and robust. Moreover, the two methods are found to be complementary with respect to the channel height. Only the manipulation of particles with negative-DEP is demonstrated in the experiments, and the throughput values up to 10^5 particles/min is reached in a continuous flow. The experimental results are compared with the simulation results and the limitations on the fabrication techniques are also discussed.

Keywords:
Dielectrophoresis / Mechanical machining / Microfluidics / 3D Sidewall electrodes
DOI 10.1002/elps.201400486

Additional supporting information may be found in the online version of this article at the publisher's web-site

1 Introduction

When the fabrication of microfluidic devices is concerned, there are basically two common approaches that are direct substrate manufacturing (photolithography, laser ablation, etc.) and mold-based techniques (hot embossing, injection molding, or soft-lithography) [1]. One alternative to fabricate the microfluidic device is to use mechanical machining (i.e. micro-milling) either for direct substrate manufacturing or for the fabrication of the mold [2–5]. For the direct substrate manufacturing, the limits of the process are constrained by the size of the milling tool that may lead to unsatisfactory end-product for microfluidic applications. However, for the fabrication of the mold, the limits of the process are constrained with the *xyz*-accuracy of the tool-positioner of a computer numerical control-machine, since the negative of the microfluidic structure is fabricated as the mold. Alternative to the lithography-based techniques, a mold can be fabricated using mechanical machining in the order of hours within the

Correspondence: Professor Barbaros Çetin, Mechanical Engineering Department, Microfluidics and Lab-on-a-chip Research Group, Bilkent University, Ankara 06800, Turkey
E-mail: barbaros.cetin@bilkent.edu.tr, barbaroscetin@gmail.com
Fax: +90-312-266-4126

Abbreviations: AC-DEP, alternating current dielectrophoresis; **CAM**, computer aided manufacturing; **DC-DEP**, direct current dielectrophoresis; **DEP**, dielectrophoresis/dielectrophoretic; **HM**, hybrid method; **MMM**, mechanical machining-based method; **nDEP**, negative dielectrophoresis; **pDEP**, positive dielectrophoresis; **WEDM**, wire electric discharge machining

Colour Online: See the article online to view Figs. 1–4 in colour.

desirable accuracy limits for microfluidic devices without any need for clean-room equipment. In the case of micro-milling, metal-based materials (such as titanium, stainless steel, etc.) as well as polymer-based materials (such as plexiglass) can be used as the mold material, which are superior to silicon or photo-resist based mold materials in terms of the durability and robustness.

Dielectrophoresis (DEP) is the movement of particles in a non-uniform electrical field due to the interaction of the particle's dipole and the spatial gradient of the electrical field. It is a label-free method to manipulate particles at microscale using the particles' inherent electrical properties. Depending on the electrical properties of the particles and the suspending medium, and on the frequency in the case of AC field, DEP can induce either negative or positive force on the particle [6]. DC-DEP, AC-DEP, and DC-biased AC-DEP have been successfully implemented for the manipulation of micro/nanoparticles within the microfluidic devices [6, 7]. For dielectrophoretic applications, usually metal structures (used for electrodes) are required that are designed and located strategically within the microfluidic structure to create the required non-uniform electric field and the required DEP force. As a common practice, electrodes are planar that are normally in the form of thin film metal layer (thickness$< 1 - 2\ \mu$m) patterned on the bottom floor of a microchannel [6]. Fabrication process consists of photolithography, thin film deposition and lift-off. Alternatively, a thin metal layer could be patterned directly in the absence of photolithography and etching by using laser ablation or deposition via a shadow mask [8, 9]. Such planar electrodes generate a fringe-like electric field and make the DEP force effective in the vicinity of the electrodes [6]. One alternative to this issue is to use 3D electrode structures at the sidewalls. With such a configuration, uniform DEP force field in the height direction can be generated. 3D sidewall electrodes may generate an effective DEP force in the lateral direction to the flow for the entire height of the device that is very convenient for continuous flow separation devices. By the use of taller microchannels, the throughput of the device can be increased.

Despite the advantages associated with 3D sidewall electrodes, fabrication of vertical electrodes requires considerable challenge and effort. Regarding this importance, different 3D electrode fabrication techniques for DEP applications have been developed and presented [10–27]. Iliescu et al. [10] proposed using highly doped silicon as a 3D electrode, and managed to separate viable and nonviable yeast cells [11]. Wang et al. [12] proposed the fabrication of 3D electrodes at the sidewalls by electroplating, and utilized this structure for flow cytometry [13] and continuous separation of human-kidney cells and N115 mouse-neuroblastoma cells by AC-DEP [14]. Wang et al. [26] also presented a DEP device with vertical electrodes that was fabricated for multiplexed switching of objects. The device was employed for manipulating coupled DEP forces, and particles flowing in a microchannel could be positioned at appropriate equilibrium positions to flow out to different outlets (up to five outlets). Kang et al. [15], and Cetin et al. [16, 17, 28] fabricated 3D copper electrodes with an extended-photolithography technique and embedded them along the sidewalls to implement the continuous separation of polystyrene particles and cells by size [15, 16] and by electrical properties [17]. Demierre et al. [18] proposed using side channels (what they called "access channels") filled with buffer solution and in touch with the electrodes to shape the electric field in 3D without any need for an additional 3D electrode fabrication step. They utilized focusing microparticles [18], and sorting viable and nonviable yeast cells [20, 21] by this design. Zhang et al. [19] utilized titanium micromachining and multilayer lamination method for the fabrication of DEP devices with floor and sidewall electrodes. Floor electrode device was utilized for size-based separation of polystyrene spheres. Moreover, sidewall electrode device was used for Z–dimension flow visualization of polystyrene particles for negative DEP (nDEP) and positive DEP (pDEP) analysis. Martinez-Duarte et al. [22] and Jaramillo et al. [29] proposed the use of 3D carbon electrodes fabricated by C-MEMS technique for superior filtering efficiency. Use of carbon electrodes also minimized the possibility of electrolysis since carbon is chemically more stable than metals. They successfully trapped yeast cells from the mixture with polystyrene particles [22], and *E. Coli* bacteria from a mixture with *B. cereus* bacteria [29]. Lewpiriyawong et al. [23] proposed the use of conductive PDMS (the PDMS was mixed with gold-powder to make it conductive) as 3D sidewall electrodes, and utilized AC-DEP for the continuous separation of 10 and 15 μm polystyrene particles. Ion-implantation technique was utilized for patterning of 3D electrodes in a microfluidic device [24]. The proposed device was implemented for electro-orientation within the microchannel to align the bacteria to the electric field, and to move the particles towards the middle of microchannel with functionality in combining large microchannels with smaller structures. In order to create electrodes on the walls of microchannel, the ions were implanted at a specific angle. Li et al. [25] proposed a technique to construct arc-shaped, 3D electrodes at the microchannel wall by utilizing low melting point bismuth alloy (melting point is around 47°C). Bismuth microspheres were produced using a specific device and were positioned at the sidewall. To show the application of presented microfluidic device, manipulation of particles, and cell-particle and particle–particle separation were conducted using DEP. More recently, Nasabi et al. [30] presented a microfluidic device for trapping viable yeast cells using 3D semi-spherical microelectrodes fabricated by the combination of soft lithography and standard photolithography. In addition to experimentation of proposed device, numerical simulation was performed for semi-spherical 3D electrode configuration. Both simulation and experimental results have shown the efficiency higher than 90% for semi-spherical 3D electrode configuration compared to planar electrodes. More information about the fabrication techniques of DEP devices for particle manipulation and separation can be found in two recent review articles [8, 31].

Although 3D electrodes were able to be embedded within microfluidic devices, the previous techniques had some

disadvantages such as higher voltage requirement in the case of conductive polymers [10, 11, 23] than that of the case with metal electrodes (since the conductivity of the polymers was not as high as metals) that may lead to complicated electronic circuitry when higher frequencies are needed, and low repeatability of the fabrication process [15–17, 28]. Moreover, all of them required lithography- or MEMS-based fabrication techniques that usually require clean room facilities, and many of them require precise alignment at some step of the fabrication [12, 24, 25] and/or careful handling of the device [15, 17, 19, 28]. These fabrication techniques also have a geometric limitation on the channel height and the pillar height (in the case of pillar-based systems) that is important when the throughput of the device is concerned. In this study, two alternative fabrication techniques are proposed for the fabrication of a microfluidic device with 3D sidewall electrodes namely (i) mechanical machining-based method (MMM) and (ii) hybrid method (HM). Both techniques utilize the high precision mechanical machining of the mold structure using the fabrication facility of the *Bilkent University Micro System Design and Manufacturing Center*. MMM also utilizes mechanical machining of the electrode structure. On the other hand, HM uses electrode deposition by using a shadow mask that is also fabricated by electric discharge machining (WEDM). Both techniques are assessed as highly repeatable and robust. MMM and HM can produce microchannels with 3D sidewall electrodes with a height of $100 - 500\ \mu m$, and $50 - 150\ \mu m$, respectively. Only the manipulation of particles with negative-DEP is demonstrated in the experiments with different flow rates and applied voltages, and the throughput values up to 10^5 particles/min are reached in a continuous flow. The experimental results are compared with the simulation results and the limitations on the fabrication techniques are also discussed.

2 Materials and methods

In a previous study [32], it has been shown that particles could be separated based on their electric properties using AC-DEP in a continuous flow, and simulated that 3D sidewall electrodes are superior to planar electrodes considering the particle manipulation. It has also been demonstrated that symmetric electrodes with multiple small tips had better performance. In this study, two alternative fabrication techniques have been proposed for the fabrication of a microfluidic device with 3D sidewall electrodes with multiple small tips.

2.1 Mechanical machining-based method

The device is a PDMS microfluidic chip consisting of a rectangular microchannel which connects one inlet and two outlets, and has been bonded to a glass substrate ($25 \times 75 \times 1\ mm^3$) following a mold-based fabrication technique. The device has embedded and reusable electrodes. The mold is fabricated from brass, and reusable electrodes are fabricated from stainless steel using high precision mechanical machining.

2.1.1 Fabrication of the mold

Fabrication of mold with micro-features is of significant importance that directly dictates the quality of the microchannels in the microfluidic device. The fabrication process of these molds demand special attention in preparing CAM (computer-aided manufacturing) program and machining process. In the development of CAM program, adaptive feed rate control options together with interpass cleaning strategies are used. Micromilling operations are conducted on a DECKEL MAHO-HSC55 milling center equipped with NSK HES510-HSKA63 high speed spindle with a run out less than one micrometer. In order to have better control on Z-levels, the mold is mounted on a KISTLER-9256C1 mini-dynamometer. Very fine grain Tungsten Carbide micro-end mills (NS Tools-MSE230) are used for micromilling operations (the details of the machining steps can be found elsewhere [33]). Microchannel has the height of 100 μm, width of 100 μm and length of 55 mm. The depth of the microchannel cavity has been chosen as 3 mm. Figure 1A shows the fabricated brass mold. Microscopic images of different regions of mold are also provided to show the high precision machining performance. Screws in the two sides of the mold are considered to apply force and prevent the leakage of the PDMS between the tips of the electrode and microchannel. Two guide pins are considered within the mold for the ease of placement for each electrode.

2.1.2 Fabrication of the electrodes

Fabrication of electrodes consists of two separate steps: micromilling and WEDM (the details of the machining steps can be found elsewhere [33]). The profile of the tips in small electrode and external contours are cut by Sodik-AP250L WEDM machine. A Zinc coated Brass wire of 0.1 mm in diameter is used. In WEDM process, the performance of cutting depends on 17 different parameters. A user defined data base is created to machine electrodes to attain the best accuracy and surface finish by adjusting main EDM parameters (Supporting Information Table S-1 illustrates the values of main adjustable parameters together with the description of each parameter). A stainless steel sheet of 1 mm thickness has been utilized for the manufacturing of asymmetric electrodes. Large electrode is 9 mm in length and 5 mm in width. The small electrode has five tips with a length of 150 μm and the same width as the large electrode. The space between tips in small electrode is 1 mm. The fabricated electrodes are presented in Fig. 1B. 3D microscopic images confirm the good surface quality of electrodes in the regions that would be in contact with microchannel wall.

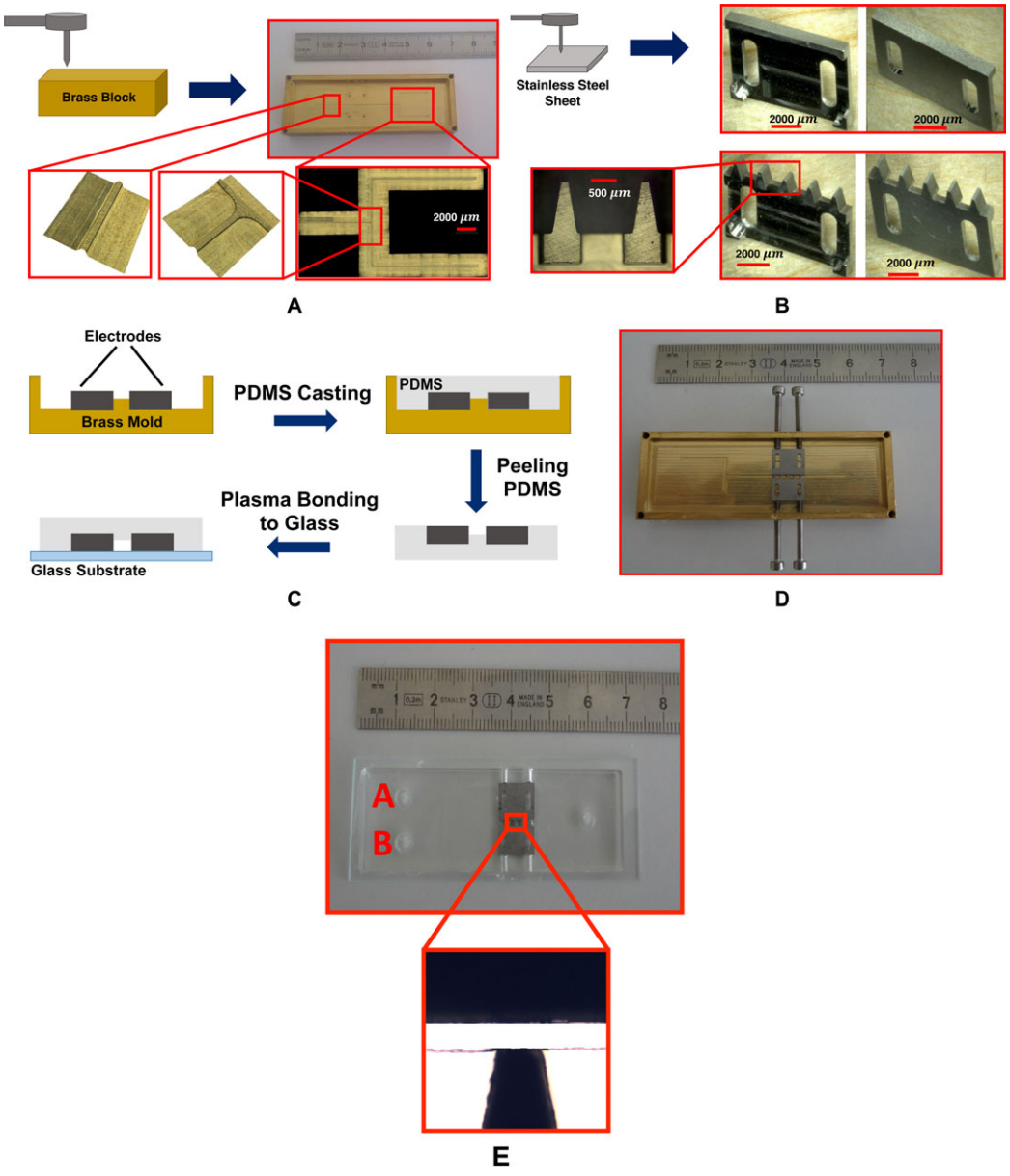

Figure 1. (A) Fabricated brass mold and the microscopic images, (B) fabricated small and large electrodes, (C) assembly of the electrodes and mold, (D) the fabrication process, and (E) the final device.

2.1.3 Assembly of the device

Electrodes are placed at the desired locations of the mold by the aid of the guide pins. The screws at the side wall are tightened to apply pressure at the interface between the electrodes and the microchannel sidewalls to prevent the leakage of the PDMS into the interface. PDMS and curing agent are mixed in the ratio of 10:1, and poured into the mold. The device is placed in an oven to cure the PDMS (75°C for 90 min). Screws and upper plate are removed from the system. PDMS is peeled off from the mold. The reservoirs are punched out, and a clean glass slide and the PDMS are plasma treated for the bonding. Fabrication steps are summarized in Fig. 1C. Assembly of electrodes and mold is presented in Fig. 1D, and the microfluidic device with reusable, embedded, 3D electrodes is shown in Fig. 1E.

2.2 Hybrid method

The device is a PDMS microfluidic chip consisting of a trapezoidal microchannel (i.e. with tilted sidewalls) that connects one inlet and two outlets and has been bonded to a glass substrate ($25 \times 75 \times 1$ mm^3). The device has 3D, deposited sidewall electrodes.

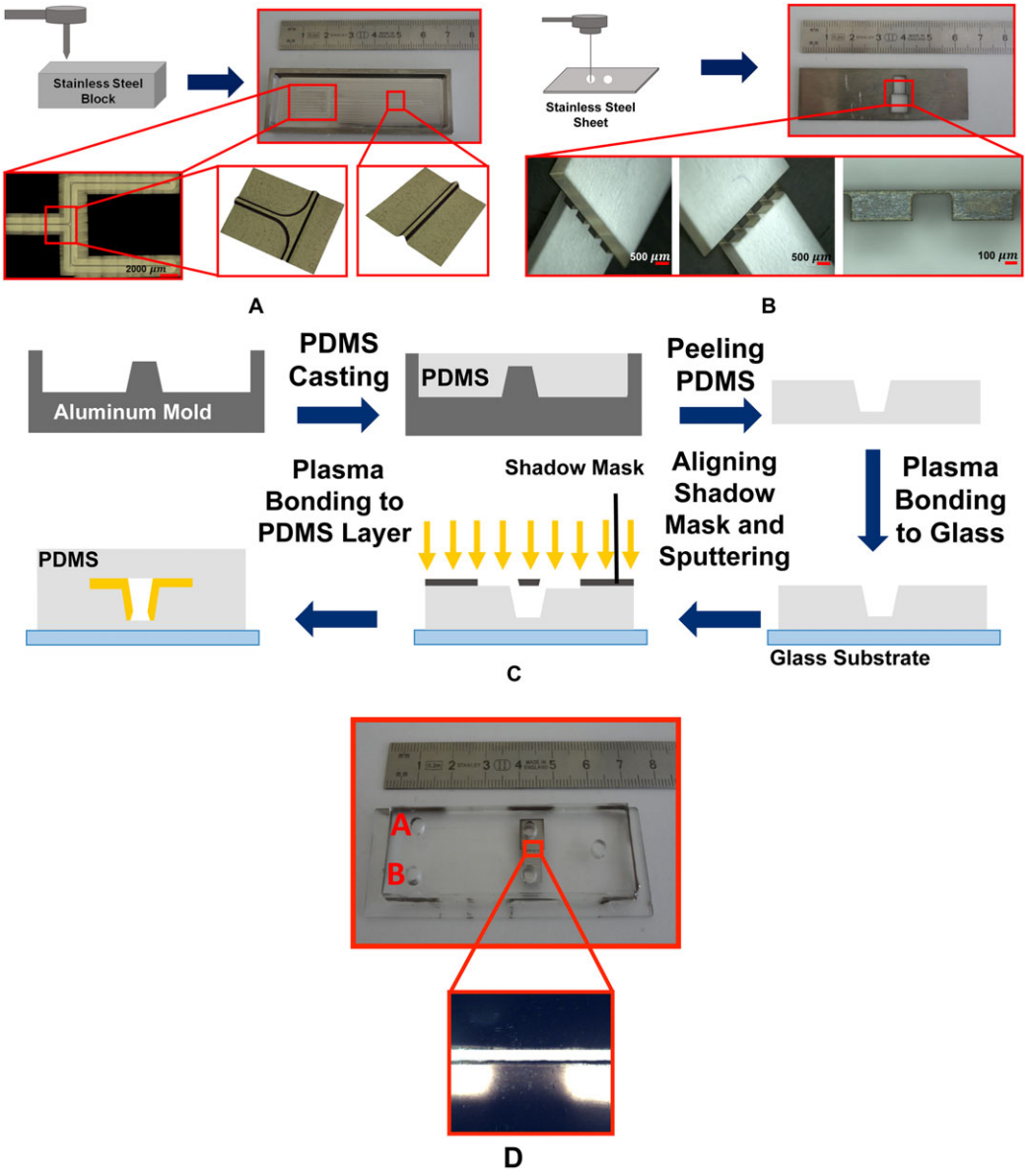

Figure 2. (A) Fabricated stainless steel mold and the microscopic images, (B) fabricated shadow mask and the microscopic images, (C) the fabrication process, and (D) the final device.

2.2.1 Fabrication of the mold

The mold is fabricated from stainless steel using high precision machining. Trapezoidal microchannel profile has been preferred for this mold in order to be able to generate deposited metal layer in the microchannel wall that provides 3D sidewall electrode configuration for the device. Fabrication of the mold is conducted with the same milling center (the details of the machining steps can be found elsewhere [33]). The microchannel has the same dimensions with that of fabricated by MMM. Figure 2A shows the fabricated stainless steel mold. Microscopic images of different regions of mold are also provided to show the high precision machining performance.

2.2.2 Fabrication of the shadow mask

Specific electrode pattern has been generated by implementing sputtering and metallic shadow mask that has the required durability to be used in the box coater. High precision machining of stainless steel sheet (0.8 mm-in-thickness) is hired for fabrication of shadow mask. WEDM machine is used for shadow mask fabrication. Due to the very tiny feature in the middle of the shadow mask, it is very susceptible to be burnt off; therefore, an optimum set of WEDM parameters are essential. Shadow mask has two grooves resembling small and large electrodes configurations. The groove that represents large electrode is in shape of rectangle with 6 mm in length and 7 mm in width. The other groove consists of five

tips with length of 400 μm and represents small electrode and has the same width with the groove of the large electrode. The minimum distance between the grooves is 40 μm. Figure 2B illustrates fabricated shadow mask by using WEDM.

2.2.3 Fabrication of the device

Following the fabrication of the mold and shadow mask, PDMS, and curing agent are mixed in the ratio of 10:1, and poured into the mold. At this step, special care is taken to prevent any air trap in the polymer, especially regions around the microchannel. The device is placed in an oven to cure the PDMS (75°C for 90 min). PDMS is peeled off from the mold. A clean glass slide and the back side of PDMS plate are plasma treated, and bonded. Shadow mask is gently and accurately aligned on the PDMS plate, such that the thin feature between two grooves of mask locates exactly in the middle of microchannel. The assembled setup is taken to the box coater and 500 nm Cr is deposited on the device using sputtering technique. The shadow mask is separated from the PDMS plate. A PDMS layer with punched out reservoirs is prepared and is bonded to the glass/PDMS sandwich using plasma treatment for fabrication of final microfluidic device. Fabrication process of the microfluidic device with 3D, deposited electrodes and the photograph of final device are presented in Fig. 2C and D, respectively.

2.3 Assessment of the fabrication techniques

Two fabrication processes have been described for the fabrication of microfluidic device with 3D sidewall electrodes. The advantages offered by the proposed fabrication techniques could be listed as:

- Fabricated molds could be used for many times without any damage.
- Fabrication of a mold with tilted sidewalls and/or with varying channel height is possible without any major complication.
- Machined electrodes are reusable and could be safely removed from the chip before disposing.
- Device assembly is straightforward and does not require any specific device or tool.
- Fabrication of the microfluidic devices could be performed in standard laboratory environment, no clean-room environment and facilities are required.
- Unique design of reusable electrodes provides robust bonding between PDMS layer and glass substrate, and prevents any leakage of fluid while pumping through the microchannel.
- Fabricated shadow mask is robust and durable, and could be used many times.
- Fabrication of device with deposited electrode provides possibility of fabricating finer electrode structures.
- Fabrication processes are highly repeatable and reproducible.
- Fabrication processes are time and cost-effective with microchannel structures without sharp edges.

In the fabrication of devices, there are some points that should be considered for the devices with good functionality. During insertion of the reusable electrodes, the tightening of screws at the sides of the mold should be performed gently to maintain the channel wall from tip print of small electrodes. In fabrication of the device with deposited electrodes, the shadow mask should be aligned on the PDMS layer such that the thin feature being in the center of microchannel guarantee the deposition of metal layer on the microchannel sidewall. The acute angle in trapezoidal microchannel has been chosen as 76° that enables the deposition of the metal on the sidewalls, and yet prevents the deposition of the electrodes on the bottom wall by the help of the tiny feature in the middle of the shadow mask.

Considering the geometrical limits of the fabrication, the height of microchannel needs to be larger than 100 μm due to the ease of placement of the electrodes and the device assembly for MMM. Although it has not been demonstrated, MMM is less problematic for the channels with the height higher than 100 μm, and it has been observed that the height of the channel can easily reach up to 500 μm during the in-house trials. For HM, the fabrication may be problematic as the height goes below 50 μm and above 150 μm due to the difficulty associated with placing the shadow mask, and it may be difficult to obtain the desired geometry. Therefore, depending on the desired channel height of a microfluidic device, the appropriate fabrication technique may be chosen. It can be concluded that both fabrication processes are robust and highly reproducible, and the channel structure is also robust and withstands high flow rates up to 50 μL/min for the prescribed cross-sections.

3 Results and discussion

The aim of the experimentation is to demonstrate the manipulation of 5 μ*m* latex particles with nDEP force, in other words pushing toward the large electrode and collecting in Reservoir A (referring to Fig. 1E and D) located at the same side with the large electrode. A 5 μm diameter latex particles (Latex Spheres BCR–Certified reference material by InterLab Inc.) with a mass concentration of 2 g/mL are used to examine the device feasibility and performance for the manipulation of nDEP particles. Specific value of particle solution is washed by DI water to prevent contamination and the sticking of the particles on the channel walls. Following the washing, the particles are suspended in a specific amount of buffer solution with conductivity of 360 μS/cm that is measured by using conductivity meter (HANNA Instruments, HI 9812-5). Laboratory syringe pump (New Era Pump Systems-NE 300) is used to load the bulk solution from inlet reservoir through the microchannel, and flexible and transparent tubes with inner

diameter of 3 mm have been implemented as the interface of the syringe pump and the inlet hole. A function generator (AGILENT 33250A) has been used to generate square waves with specific voltage and frequency. In order to produce required voltages in higher frequencies, an amplifier (Falco Systems WMA-300) has been located in the electrical manipulation circuit. The particle motion is monitored by an optical microscope (K3DI 3D Microscope Converter System by AIV Labs).

3.1 Device fabricated by MMM

The experiments with microfluidic device fabricated by MMM are started by the placement of metal pins as electrical connection interface, attaching flexible tube, and aligning the device under the microscope objective. In order to check the flow symmetry through the microchannel, applied voltage, and frequency are switched off and the syringe pump is switched on at a specific flow rate. The symmetry of the flow in the microchannel ensures the manipulation of the particle motion as a result of the DEP force. Prior to each experiment, the flow symmetry is checked with the electric field off. Afterwards, the electrical field is switched on to observe the particle manipulation. The electric field is switched on and off three times to check the repeatability of the results, and particle trajectories are recorded during the last run. During the first set of experiments, the camera is adjusted to record 15 frames per second and a video is recorded for 30 s. To generate the figures, the frames are superimposed on each other. However, for the clarity of the figures, only 50 frames are used among 150 frames (so only one frame out of every three frames is taken).

In the first set of the experiment, to analyze the n-DEP response, applied voltage and frequency are adjusted to be fixed at 10 V_{pp} and 3 MHz, respectively. This frequency is found to provide nDEP response [33]. Buffer solution with a particle concentration of 6×10^6 particles/mL is used in this set of experiments. Figure 3A shows the particle trajectory within the microchannel without any electrical field. It is observed that without any electrical manipulation, bulk solution flows in the microchannel with full symmetry. This procedure is repeated at different flow rates. Figure 3 shows the resultant experimental results. Figure 3B shows the results for the flow rate of 0.2 μL/min with an applied voltage of 10 V_{pp}. As seen from the figure, all of the particles are directed in to the Reservoir A under the action of nDEP force. Figure 3C shows the results for the flow rate of 0.5 μL/min with an applied voltage of 10 V_{pp}. Since the flow rate is increased, the DEP force is not strong enough to manipulate all the particles (the time which particles are exposed to the DEP force decreases with the increasing flow rate). The number of the particles directed towards the Reservoir A is determined by the visual inspection of the video frames. Only 85% of the incoming particles are directed toward the Reservoir A. Figure 3D shows the results for the flow rate of 1.0 μL/min with an applied voltage of 10 V_{pp}. In this case, the percentage of the particles directed toward Reservoir A decreases more, and approximately 65% of the incoming particles are manipulated. The percentage of the particles is obtained by the visual inspection of the recordings. The percentage of the incoming particles that are manipulated can also be used as the manipulation efficiency.

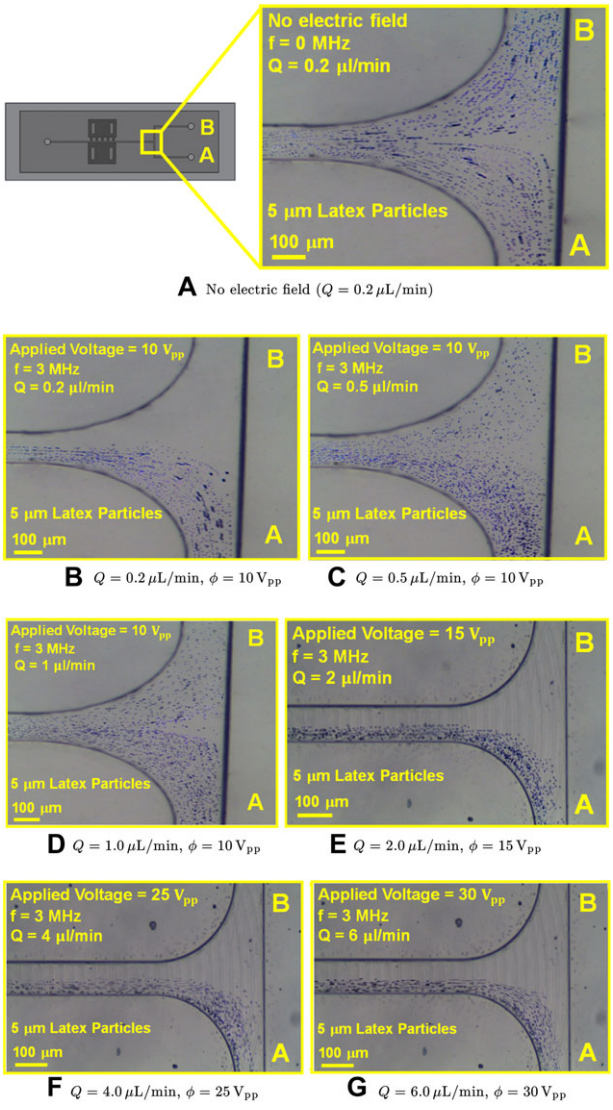

Figure 3. Particle trajectories within the microfluidic device fabricated by MMM: (A) No electric field ($Q = 0.2$ μL/min), (B) $Q = 0.2$ μL/min, $\phi = 10$ V_{pp}, (C) $Q = 0.5$ μL/min, $\phi = 10$ V_{pp}, (D) $Q = 1.0$ μL/min, $\phi = 10$ V_{pp}, (E) $Q = 2.0$ μL/min, $\phi = 15$ V_{pp}, (F) $Q = 4.0$ μL/min, $\phi = 25$ V_{pp}, (G) $Q = 6.0$ μL/min, $\phi = 30$ V_{pp}.

In the second set of experiments for this device, higher flow rates are considered to be employed with specific values of applied voltage to obtain complete collection of particles in Reservoir A (i.e. 100% manipulation efficiency). Buffer solution with a particle concentration of 2×10^7 particles/mL is used in this set of experiments. Three different flow rates are considered: 2.0, 4.0, and 6.0 μL/min. Figure 3E through G shows the particle trajectories for each case. The minimum applied voltage value for obtaining complete separation in each flow rate is mentioned in the figures. Since the flow rate of the flow is increased, higher applied voltages are required

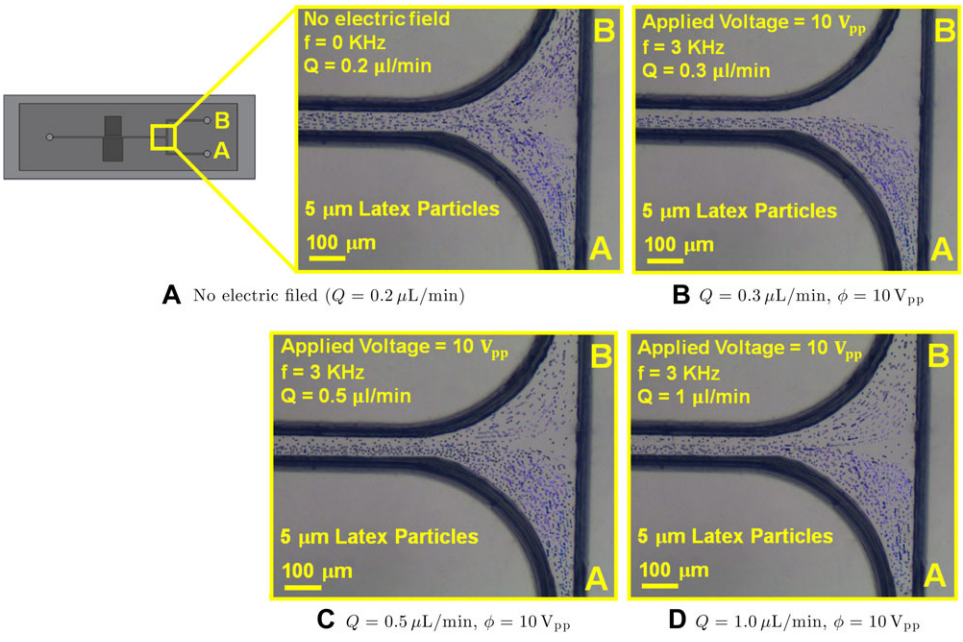

Figure 4. Particle trajectories within the microfluidic device fabricated by HM: (A) No electric field ($Q = 0.2$ µL/min), (B) Q=0.3 µL/min, ϕ=10 V_{pp}, (C) Q=0.5 µL/min, ϕ=10 V_{pp}, (D) Q=1.0 µL/min, ϕ=10 V_{pp}.

for the manipulation of the particles. The average exposure time of the particles to the electric field is 1 s that would minimize any adverse effects of the electric field.

3.2 Device fabricated by HM

Prior to the experiments, the holes above the electrodes are filled with conductive epoxy to maintain the metal thin layer and to provide durable interface for electrical connections. The same metal pins are attached to the device as electrical connection interface of manipulation circuit and microfluidic device. Buffer solution with a particle concentration of 6×10^6 particles/mL is used in this set of experiments. The same experimental procedure and image processing is followed. Applied voltage and frequency are fixed at 10 V_{pp} and 3 MHz, respectively. Figure 4A illustrates the particle trajectories without the electrical field. The symmetric flow field can be observed. After obtaining a symmetric flow through the microchannel, electric field is switched on and then particle trajectories are recorded at different flow rates. Figure 4 shows the resultant experimental results. Figure 4B shows the results for the flow rate of 0.3 µL/min with an applied voltage of 10 V_{pp}. As seen from the figure, all of the particles are directed in to the Reservoir A under the action of nDEP force. Figure 4C shows the results for the flow rate of 0.5 µL/min with an applied voltage of 10 V_{pp}. As expected, not all of the particles are directed toward the Reservoir A, and only 90% of the incoming particles are directed toward the Reservoir A. Figure 4D shows the results for the flow rate of 1.0 µL/min with an applied voltage of 10 V_{pp}. In this case, the percentage of the particles directed toward Reservoir A is approximately 80%. The manipulation efficiency of the device fabricated by HM is found to be higher than that of fabricated by MMM. The reason is that since the device fabricated by HM has trapezoidal cross-section, the electrode spacing is smaller at the bottom of the microchannel which generates higher DEP force a for a given voltage.

3.3 Assessment of the manipulation efficiency

The manipulation efficiency of the devices is also simulated using previously developed computational model [32]. The particle trajectory of polystyrene, spherical particles are simulated using COMSOL Multiphysics by point particle approach [34]. For simulation, the flow and electric fields are computed within the microchannels with the specified dimension for each device. Electric field is computed using Electric Currents Physics with specific boundary conditions. The flow field is calculated by using Laminar Flow Physics with specific boundary conditions. After obtaining electric and flow field in the microchannels, particle trajectories are obtained by using streamline function of COMSOL in postprocessing step. In order to have a random distribution of particles from the inlet, the initial locations of particles at the inlet are assigned by using normal distribution function of MATLAB via COMSOL-MATLAB interface. A mixture of 500 pDEP ($f_{CM} = 1.0$) and 500 nDEP ($f_{CM} = -0.5$) particles is released from inlet reservoir, and number of particles collected in outlets A and B are determined for both devices (A representative figure is shown in Supporting Information Fig S-2 for the clarity of the figure particle trajectory of 100 particles are shown for each device).

Table 1 shows the comparison of the manipulation efficiency obtained from the simulations with the experimental values (high throughput values also presented for HM device). As seen from the results, the simulation results agree quite well with the experimental findings that concludes that

Table 1. Comparison of the manipulation efficiency

	Manipulation efficiency (MMM)				Manipulation efficiency (HM)			
	Simulation		Experiment		Simulation		Experiment	
	nDEP	pDEP	nDEP	pDEP	nDEP	pDEP	nDEP	pDEP
$Q = 1\ \mu L/min$ $\phi = 10\ V_{pp}$	70%	62%	65%	–	80%	85%	62%	–
$Q = 0.5\ \mu L/min$ $\phi = 10\ V_{pp}$	88%	85%	85%	–	95%	85%	90%	–
$Q = 0.2\ \mu L/min$[a] $\phi = 10\ V_{pp}$	100%	100%	100%	–	100%	100%	100%	–
$Q = 2\ \mu L/min$ $\phi = 15\ V_{pp}$	100%	100%	100%	–	100%	100%	–	–
$Q = 4\ \mu L/min$ $\phi = 25\ V_{pp}$	100%	100%	100%	–	100%	100%	–	–
$Q = 6\ \mu L/min$ $\phi = 30\ V_{pp}$	100%	100%	100%	–	100%	100%	–	–

a) For HM device, $Q = 0.3\ \mu L/min$ for this case.

the proposed computational model can predict the device performance quite accurate. In the experiments, device manipulation efficiency is just examined for nDEP particles. Due to the good agreement between simulation and experiment results, it is likely to obtain similar experimental results for pDEP particles via the proposed device based on the simulation results. The simulation results for pDEP particles are also included in Table 1.

3.4 Assessment of the throughput

The development of microfluidic and LOC devices is going toward the miniaturization of biological platforms. Higher throughput, easier fabrication technique and lower fabrication costs would contribute to the mass production of disposable chips, and are beneficial for various applications including point-of-care diagnostics, drug delivery, and cellular process studies [8]. Considering the importance of device throughput in clinical and biological applications, variety of techniques have been reported for the development of high-throughput dielectrophoretic devices to manipulate and separate particle in aqueous solution. Considering the trapping-based sorting and separation devices, high throughputs have been reported. However, continuous flow systems possess some advantages over the trapping-based systems. During the trapping process, particles are exposed to the electric field that may have adverse effects on bio-particles. Moreover, the electric field within the trapping zones is affected by the accumulation of the particles that may deteriorate the trapping efficiency over time when the number of particles within the sample is high. On the other hand, in the case of continuous flow, the particles are manipulated within the flow, and the particles are exposed to the electric field for a very short duration. Moreover, the sorting and/or separation units can be integrated with other units for a complete analysis system. However, the throughput of the continuous flow devices reported is not as high as that of the trapping-based devices.

In many studies, the throughput of the device has not been reported, and only in a few studies, the throughput of the device has been reported. Cheng et al. [35] proposed a continuous microfluidic bio-particle sorter based on 3D traveling wave DEP (twDEP) that offers highest throughput of 10^4 particles/min in maximum flow rate of 10 μL/min. Similarly, Driesche et al. [36] presented continuous separation of suspended-grown biological cells implementing twDEP. PDMS layer is bonded to a glass with deposited electrodes. The highest throughput obtained by the device is 10^4 particles/min in maximum flow rate of 0.25 μL/min. Suehiro et al. [37] implemented stainless steel electrodes and glass beads of 200 μm in diameter to provide a filter in microchannel and obtain a device implemented for cell trapping with cell concentration of 10^6cells/mL and flow rate of 1000 μL/min. The bulk solution is injected into the channel with a high flow rate, and the velocity decreases as the particles pass through the manipulation region that provides high efficiency trapping of particles. Zellner et al. [38] reported insulator-based DEP microfluidic device for trapping *E. Coli* from water samples. Capture efficiency of 100% is obtained in flow rate of 6.67 μL/min with particle concentration of 10^5 particle/μL.

The throughput of the process can be obtained by multiplying the flow rate with the number concentration that gives a throughput value of 1200 particles/min, 3000 particles/min and 6000 particles/min for the cases shown in Fig. 3B through Fig. 3D, respectively. In the second set of the experiments, the throughput values of the each run is about 4×10^4 particles/min, 8×10^4particles/min, and 1.2×10^5 particles/min, respectively. The throughput of the device fabricated by HM is obtained as 1800 particles/min, 3000 particles/min, and 6000 particles/min for the cases shown in Fig. 4B through Fig. 4D, respectively. All the throughput values are also verified by the visual inspection

Table 2. Comparison of throughput of different continuous flow dielectrophoretic microfluidic devices

	Throughput (particles/min)	Flow rate (μL/min)
Cheng et al.	10^4	0.25
Driesche et al.	10^4	10
Present study	1.2×10^5	6

of the video frames. Actually, 100% manipulation efficiency can be achieved as long as the required voltage is applied. However, the applied voltage needs to be chosen to avoid any adverse effects of Joule heating. The maximum throughput value of the proposed system is compared with the continuous flow devices in the literature in Table 2. As seen from the table, a higher throughput value compared to the literature is achieved with the proposed device with 3D sidewall electrodes. Moreover, as discussed in Section 2.3, the height of the channel can be further increased, which would enhance the flow rate and the throughput for the given range of average velocity within the microchannel. Therefore, it can be concluded that with the proposed device fabricated by MMM, throughput values around 10^6 particles/min is achievable. High throughput value is important when dielectrophoretic-based manipulation is integrated with hydrodynamic and/or acoustic-based manipulation (which may reach throughput value of 10^{11} particles/min [2]). The microfluidic device fabricated by HM has not been tested for the high-throughput; however, simulations are run to predict the manipulation performance of the device fabricated by HM and the results are tabulated in Table 1 for higher specific flow rate and voltage values. As seen form results, 100% manipulation is also achievable for the same parameters that of the device fabricated by MMM for high throughput operating conditions. The manipulation efficiency decreases with flow rate; however, the throughput of the process increases with increased flow rate. Therefore, if the lower manipulation efficiency is acceptable, the sample can be processed with higher throughput with an increased flow rate.

The throughput of the proposed device is reported depending on the manipulation of nDEP particles. Regarding the separation of nDEP and pDEP particles, the simulation results also predict the 100% manipulation of the pDEP particles. However, the motion of particles would be in different directions in the case of nDEP and pDEP applications. Therefore, the prediction of the particle motion may be affected due to the interaction of the particles with each other. This may lead to lower manipulation efficiency than the simulation results. However, this can be compensated with a slight increase in the applied voltage.

4 Concluding remarks

In this study, two alternative fabrication techniques have been proposed for the fabrication of a microfluidic device with 3D sidewall electrodes. In the device fabricated by MMM, 3D electrodes are reusable, and electrodes are inserted into the sidewall of the microchannel. The other device is fabricated by HM, and 3D electrodes are deposited on the microchannel sidewalls. In fabrication of both devices, robust, durable, and reusable molds are fabricated by high precision machining (micro milling) and can be utilized many times. In the device fabricated by MMM, electrodes are fabricated by high precision machining (micro milling and WEDM) and can freely be separated during the disposal of the device and reused in fabrication of new devices. In fabricated device by HM, a shadow mask is required to generate desired electrode configuration on the microchannel sidewalls. The shadow mask is fabricated from stainless steel sheet with high precision machining (WEDM). Like the electrodes and molds, shadow mask has also enough robustness and durability to be used many times as mask in metal deposition step. To assess the device performance, only the manipulation of particles with negative-DEP is demonstrated in the experiments, and the throughput values up to 10^5 particles/min is reached in a continuous flow. The performance of the device for the separation of nDEP and pDEP particles is assessed in terms of simulations.

Modeling of a microfluidic device with three functionality of washing, separation, and concentration of (bio)particles was performed previously [34]. In the next step, the DEP device will be integrated with acoustophoretic device to provide three functionality of washing, separation, and concentration in a unique microfluidic device. Acoustophoretic devices have higher throughput than DEP devices [2]. Thus, during the integration of DEP and acoustophoretic devices, throughput matching is of high importance. In addition, for clinical applications, device throughput needs to be higher than 10^6 particles/min [2, 39]. The proposed devices have a potential for more improvement that would enable implementation of DEP-based devices for clinical applications. In clinical platforms of DEP devices, one major issue could be thermal characteristics of the device. An efficient thermal management of device can be performed by appropriate designing of the device and the system. The implementation of the proposed device for the separation of bioparticles and integration with an acoustophoretic device will be our future research directions.

Financial support from the Turkish Scientific and Technical Research Council, Grant No. 112M102, is greatly appreciated. The authors would also like to thank Ministry of Development of Turkey (HAMIT-Micro System Design and Manufacturing Research Center)

The authors have declared no conflict of interest.

5 References

[1] Lin, Y.-S., Yang, C.-H., Wang, C.-Y., Chang, F.-R., Huang, K.-S., Hsieh, W.-C., *Sensors* 2012, *12*, 1455–1467.

[2] Cetin, B., Ozer, M. B., Solmaz, M. E., *Biochem. Eng. J.* 2014, *92*, 63–82.

[3] Cetin, B., Asik, M. D., Taze, S., *J. Nanotechnol. Eng. Med.* 2014, *4*, 031004–031004.

[4] Zeinali, S., Cetin, B., Buyukkocak, S., Ozer, B., 16^{th} Int. Conference on Machine Design and Production (UMTIK), Izmir, Turkey, 2014.

[5] Warkiani, M. E., Guan, G., Luan, K. B., Lee, W. C., Bhagat, A. A. S., Kant Chaudhuri, P., Tan, D. S.-W., Lim, W. T., Lee, S. C., Chen, P. C. Y., Lim, C. T., Han, J., *Lab Chip* 2014, *14*, 128–137.

[6] Cetin, B., Li, D., *Electrophoresis* 2011, *32*, 2410–2427.

[7] Pethig, R., *Biomicrofluidics* 2010, *4*, 022811.

[8] Li, M., Li, W. H., Zhang, J., Alici, G., Wen, W., *J. Phys. D Appl. Phys.* 2014, *47*, 063001.

[9] Tay, F. E. H., Yu, L., Iliescu, C., *DEF SCI* 2009, *59*, 595–604.

[10] Iliescu, C., Yu, G. L., Samper, V., Tay, F. E. H., *J. Micromech. Microeng.* 2005, *15*, 494–500.

[11] Yu, L., Iliescu, C., Xu, G., Tay, F. E. H., *J. Microelectromech. S.* 2007, *16*, 1120–1129.

[12] Wang, L., Flanagan, L. A., Jeon, N. L., Monuki, E., Lee, A. P., *Lab Chip* 2007, *7*, 1114–1120.

[13] Wang, L., Flanagan, L. A., Lee, A. P., *J. Microelectromech. S.* 2007, *16*, 454–461.

[14] Wang, L., Lu, J., Marchenko, S. A., Monuki, E., Flanagan, L. A., Lee, A. P., *Electrophoresis* 2009, *30*, 782–791.

[15] Kang, Y., Cetin, B., Wu, Z., Li, D., *Electrochim. Acta* 2009, *54*, 1715–1720.

[16] Cetin, B., Kang, Y., Wu, Z., Li, D., *Electrophoresis* 2009, *30*, 766–772.

[17] Cetin, B., Li, D., *Electrophoresis* 2010, *31*, 3035–3043.

[18] Demierre, N., Braschler, T., Linderholm, P., Seger, U., van Lintel, H., Renaud, P., *Lab Chip* 2007, *7*, 355–365.

[19] Zhang, Y. T., Bottausci, F., Rao, M. P., Parker, E. R., Mezic, I., MacDonald, N. C., *Biomed. Microdevices* 2008, *10*, 509–517.

[20] Valero, A., Braschler, T., Demierre, N., Renaud, P., *Biomicrofluidics* 2010, *4*, 022807.

[21] Mernier, G., Piacentini, N., Braschler, T., Demierre, N., Renaud, P., *Lab Chip* 2010, *10*, 2077–2082.

[22] Martinez-Duarte, R., III, R. A. G., Abi-Samatra, K., Madou, M., *Lab Chip* 2010, *10*, 1030–1043.

[23] Lewpiriyawong, N., Yang, C., Lam, Y. C., *Electrophoresis* 2010, *31*, 2622–2631.

[24] Choi, J. W., Rosset, S., Niklaus, M., Adleman, J. R., Shea, H., Psalties, D., *Lab Chip* 2010, *10*, 783–788.

[25] Li, S., Lim, M., Hul, Y. S., Cao, W., Li, W., Wen, W., *Microfluid Nanofluid* 2012, 499–508.

[26] Wang, L., Flanagan, L. A., Jeon, N. L., Monuki, E., Lee, A. P., *Lab Chip* 2012, *9*, 114–1120.

[27] Kilchenmann, S. C., Rollo, E., Bianchi, E., Guiducci, C., *Sensors Actuators B* 2013, 1–19.

[28] Cetin, B., Li, D., *Electrophoresis* 2009, *30*, 3124–3133.

[29] Jaramillo, M. d. C., Torrents, E., Martinez-Duarte, R., Madou, M., Juarez, A., *Electrophoresis* 2010, *31*, 2921–2928.

[30] Nasabi, M., Khoshmanesh, K., Tovar-Lopez, F. J., Kalantar-zadeh, K., Mitchell, A., *Electrophoresis* 2013, *34*, 3150–3154.

[31] Duarte, R. M., *Electrophoresis* 2012, *33*, 3110–3132.

[32] Cetin, B., Zeinali, S., 4^{th} Micro and Nano Flows Conference UCL (MNF2014), London, UK, 2014.

[33] Zeinali, S., MSc. thesis, Bilkent University, Ankara, Turkey, 2014.

[34] Cetin, B., Buyukkocak, S., Zeinali, S., Ozer, B., ASME 4^{th} International Conference on Micro/Nanoscale Heat and Mass Transfer, 2013.

[35] Cheng, I. F., Froude, V. E., Zhu, Y., Chang, H.-C., Chang, H. C., *Lab Chip* 2009, *9*, 3793–3201.

[36] van den Drieschea, S., Raoa, V., Enengl, D. P., Witarski, W., Vellekoopa, M. J., *Sensors Actuators B Chem.* 2011, *170*, 207–214.

[37] Suehiro, J., Zhou, G., Imamura, M., Hara, M., *IEEE T. Ind. Appl.* 2003, *39*, 1514–1521.

[38] Zellner, P., Shake, T., Sahari, A., Behkam, B., Agah, M., *Anal. Bioanal. Chem.* 2013, *405*, 6657–6666.

[39] Buyukkocak, S., Ozer, M. B., Cetin, B., *Microfluid Nanofluid* 2014, *17*, 1025–1037.

